Modelling and experimental analysis of the effects of run out, minimum chip thickness and elastic recovery on the cutting force in micro-end-milling

Modelling and experimental analysis of the effects of run out, minimum chip thickness and elastic recovery on the cutting force in micro-end-milling

Xiubing Jing[1], Rongyu Lv[1], Yun Chen[2], Yanling Tian[1*], and Huaizhong Li[3*]

[1]Key Laboratory of Equipment Design and Manufacturing Technology, School of Mechanical Engineering, Tianjin University, Tianjin, 300072, China

[2]Department of mechanical and electrical engineering, Xiamen University, Xiamen 361005, China

[3]Griffith School of Engineering, Gold Coast campus, Griffith University, QLD 4222, Australia

*** Corresponding author:**

Professor Yanling Tian, School of Mechanical Engineering, Tianjin University, China, E-mail: meytian@tju.edu.cn;

Dr. Huaizhong Li, Griffith School of Engineering, Gold Coast Campus, Griffith University, QLD 4222, Australia.

E-mail addresses: lihuaizhong@gmail.com;

Abstract

Prediction of cutting force has great significance for controlling the micro-end-milling processes. In this study, a mechanics model for exactly prediction cutting force is comprehensively established by considering the variety of entry and exit angles for each engaged cutting edge and an accurate instantaneous uncut chip thickness (IUCT). The determination of IUCT has considered the combination of the minimum chip thickness, tool run-out, and the material's elastic recovery, which is embedded in the cutting force model. Further, cutting force coefficients as function of uncut chip thickness have been calculated by using finite element method (FEM). To verify the reliability of the presented cutting force model, a series of experiments for cutting force are conducted and experimental results are compared to cutting force predicted. The results demonstrate that the cutting force predicted is well in agreement with that of measured. The effects of elastic recovery and tool run-out on cutting force also are investigated. Some conclusion can be drawn that elastic recovery can more obviously affect the cutting force predicted with smaller the feed per tooth, the errors of experimental and predicted is getting smaller with increasing the cutting depth, the slight change of tool run-out will lead to a great variation in cutting force.

Key word: cutting forces; mechanics model; run out; elastic recovery.

1. Introduction

The micro-milling are possessing outstanding capability of accurately producing micro-components with feature size at the order of several tens to hundreds of micrometers, which is expected to become an alternative approach for fabricating complex 3D freeform micro-component devices in various field [1]. Recently, it has been successfully applied to produce 3D microstructures in considerable kind of materials, such as titanium alloy [2], monocrystalline silicon [3], ceramics [4] and glass [5] with minimised defects.

Compared to macro machining, there are various issues in micro machining, including minimum chip thickness, flute edge radius, too run-out and plastically-elastic deformation, etc. [6], which make the mechanics of chip formation be challenging. In micro-end-milling process, the flute edge is not considered as sharp because the feed per tooth is the magnitudes of 0.5 to 5 μm, which matches the flute edge radius. Generally, the ratio of uncut chip thickness to flute edge radius is used to describe the size effect in micro milling. Moreover, the tool run-out with several micron in micro end-milling processes greatly affecting uncut chip thickness leads to the maximum cutting force increasing, which causes tool wear and dominates the tool life [7]. In the micro end milling process, the chip formation relies on the minimum chip thickness. There is no chip formation in case of the uncut chip thickness less than the minimum chip thickness, conversely, portion of the removal material occurs plastically deformation and the remaining material undergoes elastically recovery after the edge of flute passing [8]. The mechanism of chip formation leads to “size effect”, which is presented by the specific cutting force sharply increasing [9]. It is more challenging to predict the cutting forces due to above-mentioned characteristic. Therefore, it is crucial for development comprehensive cutting force models and controlling the micro milling processes.

A number of researches have conducted on developing the prediction models of cutting force in micro-end-milling process. Bao et al. [10] firstly developed prediction cutting force model for the micro-end-milling by a mechanistic method. They have calculated the instantaneous uncut chip thickness (IUCT) for mill-cutter with two flutes by considering the tool tip trajectory as trochoidal. Further, they proposed an improved IUCT model by taking into account tool run-out [11]. By incorporating the minimum chip thickness into the IUCT model, Vogler et al. [12] initially developed a mechanistic model of prediction cutting force using the slip-line theory in micro-end-milling. By considering the elastic-plastic deformation and effective rake angle, a mechanistic model of cutting force was established by Park and Malekian [13]. Jun et al. [14] proposed a precise cutting force model taking into account the tool dynamic characteristics and material’s elastic recovery in micro-end-milling process. These researches bring a phenomenon that the calculation of IUCT is very important for accurate prediction the cutting force. Actually, many newest researchers were dedicated to establish the more accurate IUCT model in micro cutting processes. Chen [15] established a more accurate IUCT model, which considered the precise trochoidal

trajectory of the cutting edge, tool runout and dynamic modulation caused by the machine tool system vibration. Yuan [16] also proposed an innovative IUCT algorithm, in which the effect of run out on the cutting tool's actual rake angle and thereof on the IUCT is analyzed. Recently, Wan [17] presented a new method to predict micro milling force considering dead metal zone together with the influence of the uncut chip thickness on micro milling force. Wojciechowski [18] focused on the prediction of cutting forces by taking into account the chip thickness accumulation during micro end milling.

There is a major limitation in the mechanistic models, which is the need for accurately calculating the cutting force coefficients through cutting calibration experiments. To overcome costly experimental limitations, finite element method (FEM) also has been used to predict the cutting forces for micro end milling. Thepsonthi and Ozel tried to establish two-dimensional FE simulation for predicting cutting force in micro milling [19]. Nevertheless, it is difficult for accurately predicting the cutting force by FEM due to limitation of higher computational power. Further, various inherent characteristics above-described affect the micro end milling process, interaction model of tool-workpiece with complex three dimension need be considered by incorporating these effects for accurate cutting force prediction.

Despite extensive research efforts devoted to establish cutting force prediction model, there is still a great gap in understanding the effect of all the relevant factor on the cutting force during micro-milling process. A comprehensive cutting force prediction still does not exist that could facilitate the industrial application and effectively monitor the micro end-milling process. To predict the accurate cutting force, above-mentioned effects, namely the minimum chip thickness, tool run-out and the elastic recovery should be incorporated the model of cutting force. The objective of this paper is to develop a mechanics model for exactly prediction cutting force taking into account tool run-out, the minimum chip thickness, and workpiece elastic recovery. The novelty of this research is to integrate the material's elastic recovery into the surfaces generated by the previously passing tool flute for calculation the IUCT in the presence of the run-out effect. In addition, the cutting force coefficients as a nonlinear function of the uncut chip thickness has been obtained by the virtual cutting experiments using FEM, which can reflect all the cutting characteristics in micro end-milling by undertaking the cutting experiment with different tool geometry and process parameters. Size effect is also included, which leads to cutting force coefficient sharply increasing. The cutting forces will, in turn, be calculated by using the cutting force coefficients and the IUCT. The proposed cutting force model will be applicable to all ductile material using calculation cutting force coefficients by FEM. This research is organized as following: a mechanistic model for cutting force considering the aforementioned effects is proposed in section 2. The experimental setup is designed to verify the proposed model and the predicted cutting force is compared with the experimental results in section 3. Finally, Section 4 obtains some conclusions.

2. Proposed Cutting Force Modelling

Prediction cutting force by mechanistic method is intend to establish in this section, which incorporates the effects of minimum chip thickness, run out and elastic recovery. A micro end-milling cutter with 2-flute and constant helical will be focused on discussing for the convenience, which is most widely utilized in micro milling.

2.1 Mechanistic model cutting force for micro-end-milling processes

Figure 1 shows a full slot micro end-milling operation with a 2-flute with helix angle micro in the Cartesian coordinate system, in which, d_a, h and ω are axial depth of cut, uncut chip thickness and spindle speed, respectively. The X- and Y- axis refer to the feed direction and cross the feed direction, respectively. Z-axis is rotational axis of the cutter. It has been reported that cutting force generated in Z-axis is comparatively low as compared to X and Y- axis in micro milling [6, 8]. In micro milling process, feature dimension is ultimately dominated by tool deflection, which is associated with cutting forces in X- and Y- directions. It has also been reported that catastrophic tool breakage occurring due to regenerative chatter is the measure of impediment [2]. Mittal et al. [20] investigated that axial force component has no significant effect on regenerative chatter and they used only tangential force coefficient to estimate chatter. Therefore, this study will consider the cutting forces in the X- and Y- direction, and cutting force in the Z-axis will be ignored.

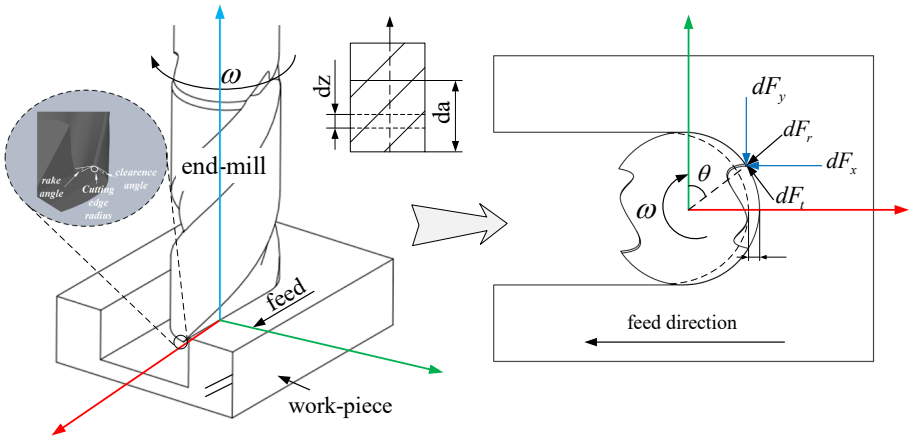

(a) Geometry and coordinate for micro end-milling (b) components of cutting force

Fig. 1 Schematic of the micro end-milling processing with helix angle

The mechanistic approach proposed by Altintas[21] is used for the development of cutting force, in which the axial depth of cut is segmented into a number of elements with equal thickness dz. Each element of cutter can be considered as a small oblique cutting with a given inclination angle. As shown in Fig. 1, the cutting force generated by the k^{th} flute for a disk of cutting dz at any rotation angle θ can be described by the tangential component (dF_{tk}) and radial component (dF_{rk}) given as [17]:

$$\begin{cases} dF_{tk}(\theta) = k_t \cdot h(\theta) \cdot dz \\ dF_{rk}(\theta) = k_r \cdot h(\theta) \cdot dz \end{cases} \tag{1}$$

where dz is the height of element of axial depth cutting; k_t and k_r are the tangential and radial cutting force coefficients, respectively, $h(\theta)$ is IUCT at rotation angle θ.

From the cutter geometry shown in Fig.1, the element of axial depth cutting dz can be written as:

$$dz = \frac{Rd\theta}{\tan\beta} \tag{2}$$

where R and β is the cutter radius and helix angle, respectively.

As shown in Fig.1, cutting force in X- and Y- directions in the Cartesian coordinate system can be deduced by transforming the tangential and radial cutting force components obtained from Eq.1, and be expressed as:

$$\begin{pmatrix} dF_{xk}(\theta) \\ dF_{yk}(\theta) \end{pmatrix} = \begin{pmatrix} -\cos\theta & -\sin\theta \\ \sin\theta & -\cos\theta \end{pmatrix} \begin{pmatrix} dF_{tk}(\theta) \\ dF_{rk}(\theta) \end{pmatrix} \tag{3}$$

Then, the resultant cutting force in X- and Y- directions acting on each engaged cutting edge can be obtained by integrating the cutting force components calculated from Eq.3, and expressed as:

$$\begin{cases} F_{xk}(\theta) = \dfrac{R}{\tan\beta}\displaystyle\int_{\theta_l}^{\theta_u} \left[-dF_{tk}(\theta)\cos\theta - dF_{rk}(\theta)\sin\theta\right] d\theta \\ F_{yk}(\theta) = \dfrac{R}{\tan\beta}\displaystyle\int_{\theta_l}^{\theta_u} \left[dF_{tk}(\theta)\sin\theta - dF_{rk}(\theta)\cos\theta\right] d\theta \end{cases} \tag{4}$$

where θ_l and θ_u are the entry and exit angles for each engaged cutting edge, respectively.

Due to the presence of the helix angle, at an axial depth of cut d_a, a point of flute will lag that of bottom by a lag angle, δ, which can be expressed as:

$$\delta = \frac{d_a \tan\beta}{R} \tag{5}$$

Cutting area by an engaged flute in one revolution can be defined as three zones named Entry, Intermediate and Exit [22]. In a full slot micro end-milling process, once the 1st flute starts exiting from the workpiece with the cutter rotation, the 2nd flute starts gradually entering due to the helix angle, which results the overlap of two successive teeth occurring [7]. The overlap zones, and corresponding entry and exit angles are shown in Figure 2, in which overlap zones is circled by red dashed frame. The total cutting force will be calculated by taking into account this overlap.

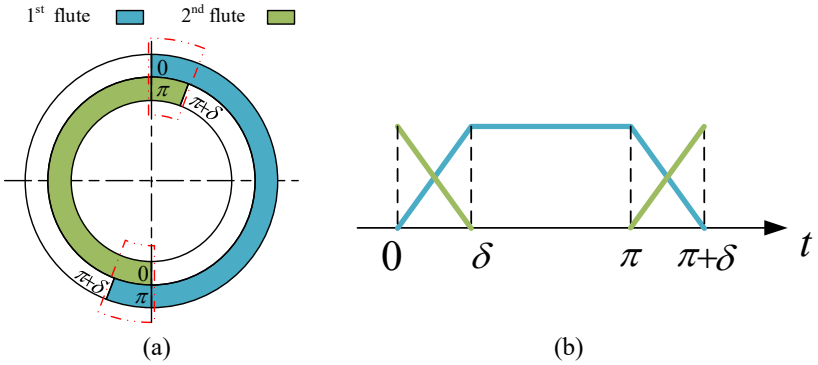

Fig. 2 three zones by helical end-mill with two flute (a) Overlap zones (b) angle for tooth engaged

Finally, the total cutting forces in X- and Y- direction can be obtained by:

$$\begin{cases} F_x(\theta) = \sum_{k=1}^{K} F_{xk}(\theta) \\ F_y(\theta) = \sum_{k=1}^{K} F_{yk}(\theta) \end{cases} \tag{6}$$

where K is the number of tooth.

Based on Eqs. (1) - (5), a series of parameters will be solved to calculate the cutting force. According the model of cutting force, the calibration of tool run-out, accurate IUCT, the cutting force coefficients will be studied in following sections.

2.2 Model for calibration of tool run-out

Since the feed per tooth is comparable to tool run-out in micro end-milling process, the effect of run out on the cutting force is not ignored. Due to the presence of tool run-out, the actual rotational radius is not identical for each flute, which leads to the chip formation by each flute be different each other. Considering the actual machining conditions, tool run-out including the axial offset and axial tilt are taken into account in this study. Figure 3 shows the model for calibration of tool run-out, in which, ρ, λ, ψ and Φ represent run out length, run out angle, tilting angle, and location angle of tilting angle, respectively. In Fig. 3(a), the centerline of the spindle and the tool are represented by O_SO_S' and O_TO_T', respectively. z_1, z_2 and z are several locations extracted from the shank of tool at different depth of cut z_1, z_2, and z along with axis. z_0 is located on the bottom of cutting edge. In Fig.3 (b), the rotational center of the spindle and the tool are represented by O_0 and O_0', respectively. Points A and B represent the tip of flute. The points of A, B and C is located on the bottom contour of tool, γ_3 is the phase difference of A and C. Moreover, C, O_0 and O'_0 are in one line.

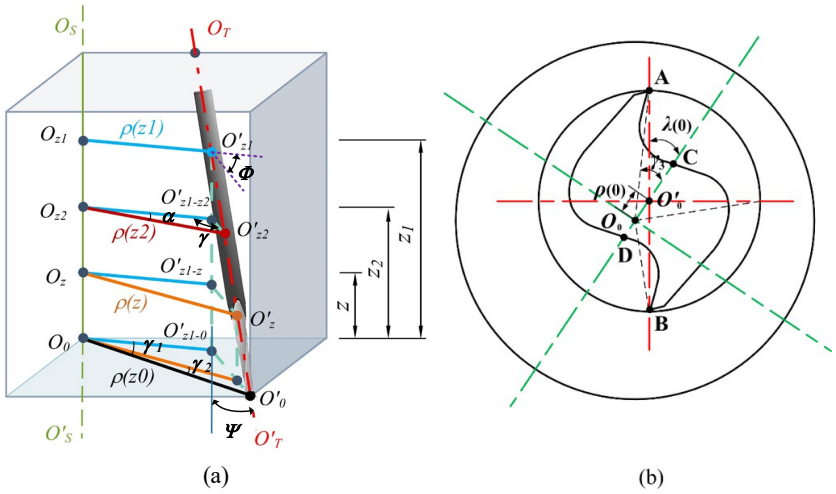

Fig.3 model of tool run-out: (a) geometry of axis offset and axial tilt. (b) Tool run-out on the bottom of cutter

From the geometric relationship in Fig. 3(a), the length of $O'z_1$-$z_2O'z_2$ can be obtained by:

$$O'_{z1\text{-}z2}O'_{z2} = \sqrt{\rho(z_1)^2 + \rho(z_2)^2 - 2\rho(z_1)\rho(z_2)\cos\alpha} \tag{7}$$

where α is the phase difference from location of z_1 to z_2, $\rho(z_1)$ and $\rho(z_2)$ are the run-out length corresponding location of z_1 and z_2, respectively. Detailed instructions for measuring $\rho(z_1)$ and $\rho(z_2)$ are available in [23]. On the basis of law of trigonometric functions, the tilt angle ψ and corresponding location angle Φ can be calculated as following.

$$\psi = \arctan\left(O'_{z1\text{-}z2}O'_{z2}/O'_{z1}O'_{z1\text{-}z2}\right) \tag{8}$$

$$\Phi = \arcsin\left(\rho(z_2)\sin\alpha/O'_{z1\text{-}z2}O'_{z2}\right) \tag{9}$$

where $O'_{z1}O'_{z1\text{-}z2}$ is the length from location of z_1 to z_2. Finally, according to the above deduced, the run out length $\rho(z)$ at different location of z can be calculated by:

$$\rho(z) = \sqrt{\rho(z_1)^2 + (z_1 - z)\tan\psi + 2\rho(z_1)(z_1 - z)\tan\tau\cos\Phi} \tag{10}$$

where z and z_1 are the height from axis location of z and z_1 to the bottom of cutter. As shown in Fig. 3(b), if, ρ, the offset distance, is obtained, corresponding λ, the offset angle, can be determined. On the bottom of cutter, namely $\lambda(0)$ is expressed as:

$$\lambda(0) = \gamma_3 + \arcsin\left(\rho(0)\sin\gamma_3/R\right) \tag{11}$$

where $\rho(0)$ is the run-out length on the bottom of cutter. By substituting z=0 into Eq. (10), $\rho(0)$ can be determined. Due to the phase lag and phase difference between the location z and the bottom of cutter, the $\lambda(z)$, run-out angle at different location z can be derived as:

$$\lambda(z)=\gamma_3+\arcsin\left(\frac{\rho(0)\cdot\sin\gamma_3}{R}\right)+\arccos\left(\frac{\rho(0)^2+\rho(z)^2-(z\cdot\tan\tau)^2}{2\rho(0)\rho(z)}\right)+\frac{z\cdot\tan\beta}{R} \tag{12}$$

2.3 Modified model for instantaneous uncut chip thickness

Precise calculation of IUCT is important for accurately predicting the cutting force proposed in section 2.1. In micro end-milling process, due to the existence of the minimum chip thickness, elastic recovery and run out, the conventional IUCT model is no longer valid. This section presents an improved IUCT model by incorporating the above-mentioned parameters. Due to the effect of tool run out, the actual trajectory of the tool tip for end-mill with K flute at an angular position is trochoidal instead of linear trajectory presenting in Figure. 4, which results uncut chip thickness be not identical for different flutes. In Fig. 4(a), the current and previous (k^{th} and k-1^{th}) flute trajectory are indicated by the solid lines with red and blue, respectively. Due to the effect of elastic recovery, the actual surface generation represented by the green dashed line deviates from trajectory of the flute. Points M and N indicate the previous flute at time t_k and current flute at time t_{k-m}, respectively. Points O_k and O_{k-m} indicate tool center at time t_k and t_{k-m}, respectively. The line MO_k intersects the actual surface generated at point N'. The theoretical IUCT, h, is equal to the length of line $M\,N'$.

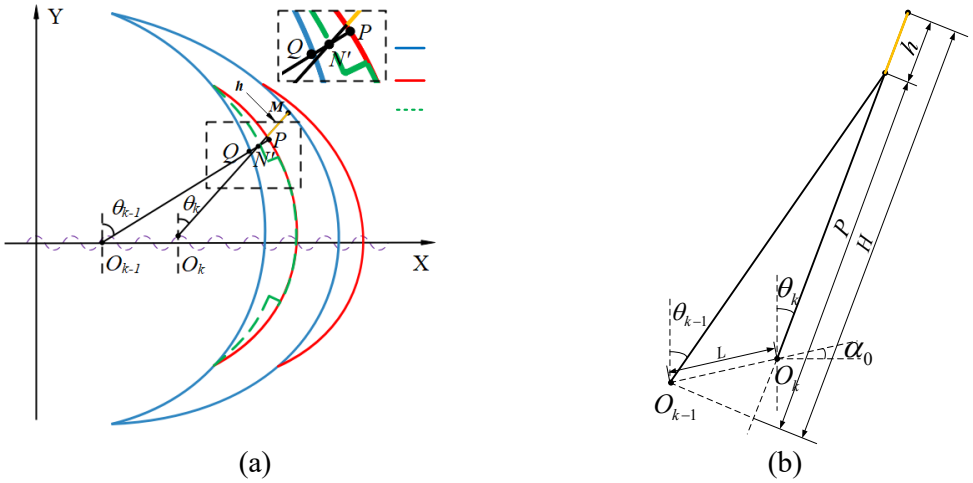

Figure 4 Model IUCT for end-mill with 2-flute (a) Trajectory of the tool tip. (b) IUCT

As shown in Fig. 4, the center position of the tool O_k and O_{k-1} corresponding at time t_k and t_{k-m}, respectively, whose coordinates can be given by:

$$\begin{cases} x(O_k)=f\,t_k/60+\rho(0)\sin(wt_k+\lambda(0)) \\ y(O_k)=\rho(0)\cos(wt_k+\lambda(0)) \end{cases} \tag{13}$$

$$\begin{cases} x(O_{k-m})=f\,t_{k-m}/60+\rho(0)\sin(wt_{k-m}+\lambda(0)) \\ y(O_{k-m})=\rho(0)\cos(wt_{k-m}+\lambda(0)) \end{cases} \tag{14}$$

Where f is feed rate (mm/min).

M point is located on the trajectory of the current flute at location angle, $\theta_k = (wt_k - 2\pi k/K)$, whose coordinates are given by:

$$\begin{cases} x(k) = R\sin(wt_k - \dfrac{2\pi k}{K}) + x(O_k) \\ y(k) = R\cos(wt_k - \dfrac{2\pi k}{K}) + y(O_k) \end{cases} \tag{15}$$

Similarly, replacing k by k-m and t_k by t_{k-m} in Eq. (15), N' point is located on the surface generated by the previous flute, whose coordinates can be obtained:

$$\begin{cases} x(k-m) = (R - P_e \cdot h_{pre}) \cdot \sin(wt_{k-m} - \dfrac{2\pi(k-m)}{K}) + x(O_{k-m}) \\ y(k-m) = (R - P_e \cdot h_{pre}) \cdot \cos(wt_{k-m} - \dfrac{2\pi(k-m)}{K}) + y(O_{k-m}) \end{cases} \tag{16}$$

Since points N', M and O_k are on the same line, the relationships can be obtained by combination Eq.15 and 16:

$$y(k-m) = \frac{x(k-m) - x(O_k)}{\tan(wt_k - 2\pi k / K)} + y(O_{k-m}) \tag{17}$$

Finally, the theoretical IUCT at location angle, θ_k can be calculated from the geometric relationships in Fig. 4(b), as following:

$$\begin{aligned} h &= H - P \\ &= (R - P_e \cdot h_{pre}) + L\sin(\theta_k + \alpha_0) - \sqrt{(R - P_e \cdot h_{pre})^2 - L^2\cos^2(\theta_k + \alpha_0)} \end{aligned} \tag{18}$$

where P_e and h_{pre} are the elastic recovery rate and height, respectively. The parameters L and α_0 are given by:

$$L = \sqrt{(x(O_k) - x(O_{k-m}))^2 + (y(O_k) - y(O_{k-m}))^2} \tag{19}$$

$$\alpha_0 = \arctan\left(\frac{y(O_k) - y(O_{k-m})}{x(O_k) - x(O_{k-m})}\right) \tag{20}$$

The chip formation mechanisms in micro-end-milling process is shown in Figure 5, in which, r_e refers to the flute edge radius. In Fig.5 (a), when the uncut chip thickness is lower than the minimum chip thickness, in which no chip formation occurs, at the same time part of material produce plastically deformation, and the remaining material undergoes elastically recovery. In turn, in the case of the uncut chip thickness is larger than the minimum chip thickness, the whole machined material as cutting chip is fully removed, as shown in Fig. 5(b). Then, the actual IUCT h_a are given as:

$$h_a = \begin{cases} (1-P_e)\cdot h & h \le h_{min} \\ h & h > h_{min} \end{cases} \tag{21}$$

where h_{min} is the minimum chip thickness.

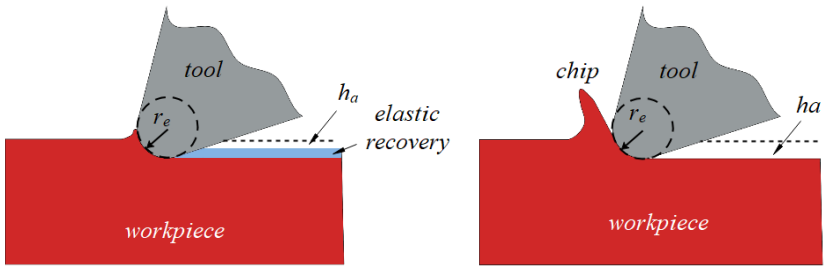

(a) No chip formation (b) chip formation

Fig. 5 Chip formation mechanisms

Hence, given these parameter of feed per tooth, tool run-out and minimum chip thickness, the actual IUCT is simulated. The minimum chip thickness is set as 0.8 μm in this study [24].

Figures 6 and 7 present the calculated IUCT by above proposed model. In Figs. 6 and 7, it can observe that IUCT for each flute is not identical due to the existence of run-out. Moreover, the total cutting angle for one flute is more than 180° while that of the other is less than 180°. For the case of the feed per tooth beyond the minimum chip thickness shown in Fig. 6, some sudden increase in IUCT for 2nd flute in Fig. 6(a)), which depends on the elastic recovery rate and run-out length, finally disappear with larger run out length in Fig. 6(b).

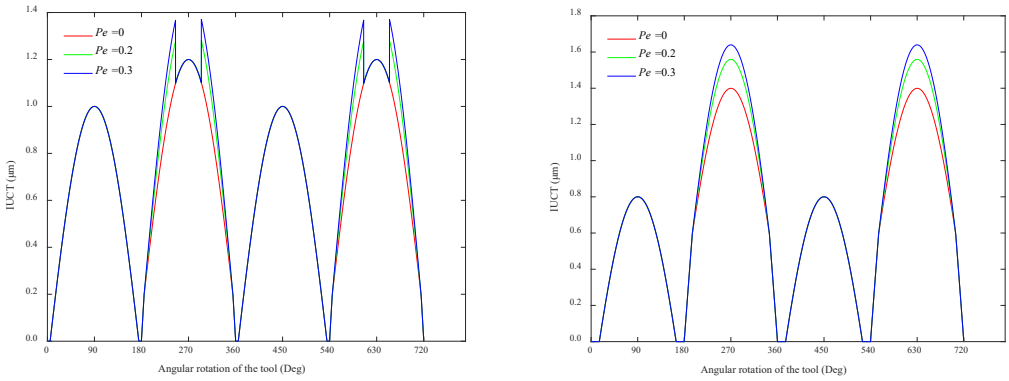

(a) 0.1 μm run-out length (b) 0.3 μm run-out length

Fig. 6 IUCT at 1.1 μm feed per tooth considering elastic recovery (3π/12 run-out angle)

Nevertheless, in Fig. 7(a), some abrupt changes appears in value of IUCT of flute 1st for the case of the feed per tooth below the minimum chip thickness, which disappears with the larger angle run-out in Fig. 7(b). It also can observe that the elastic recovery affects more significant on IUCT with smaller feed per tooth, which also is remarkable for the run-out. The elastic recovery rate effect on

the IUCT relies on the properties of the material, which can be obtained by scratch tests [25].

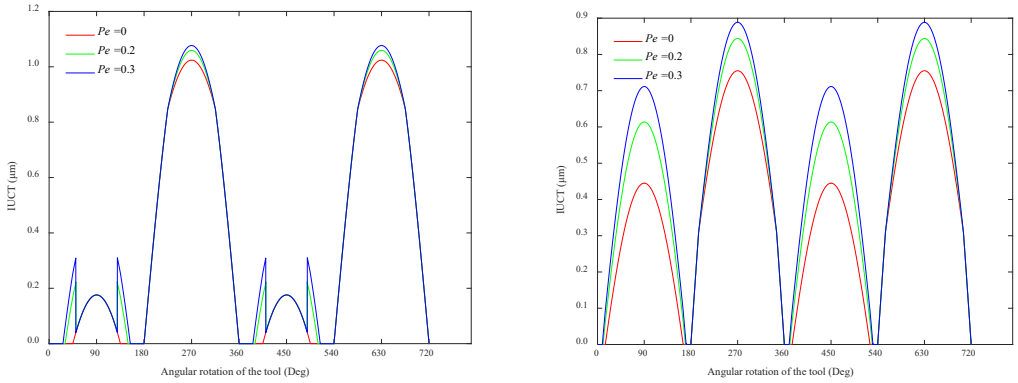

(a) 3π/12 run-out angle (b) 5π/12 run-out angle

Fig. 7 IUCT at 0.6 μm feed per tooth considering elastic recovery with 0.3 μm run-out length

2.4 Calculation of cutting force coefficients

In general, there are three methods for calculation the cutting force coefficients, including transferring orthogonal cutting to the oblique cutting, directly oblique cutting and milling [26]. Such experiments are costly and time-consuming, and gradually substituted by the virtual cutting experiments using FEM. Our previous research [27] has utilized a FEM of orthogonal cutting to obtain the cutting force coefficients, which is verified the effectiveness by experiment. Using the same approach in this study, orthogonal cutting thermo-mechanical FEM is carried out considering the edge radius by using Abaqus/Explicit 6.10. Figure 8 presents the schematic of 2-D view of the orthogonal cutting process. The workpiece is meshed based on a four-node thermo-mechanical coupled quadrilateral element, the reference point Rp is set on the tool, which is treated as pure rigid body.

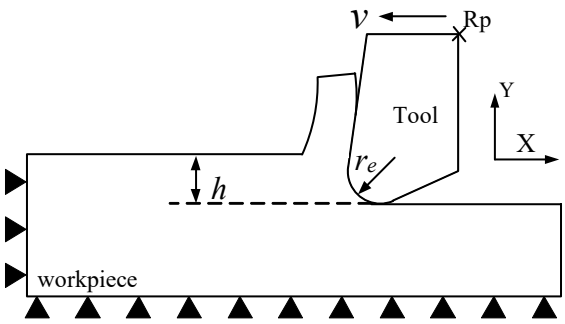

Figure 8 FE model for orthogonal cutting

The material selected in this experiment is Ti6Al4V. The workpiece is treated as elastic-plastic behavior represented by Johnson-Cook material model. Flow stress has been calculated by [28]:

$$\sigma=\left[A_1+B_1\varepsilon^n\right]\left[1+C_1\ln\frac{\dot{\varepsilon}}{\dot{\varepsilon}_0}\right]\left[1-\left(\frac{T-T_{room}}{T_{melt}-T_{room}}\right)^m\right] \tag{22}$$

where ε, $\dot{\varepsilon}$ and $\dot{\varepsilon}_0$ is the equivalent plastic strain, the equivalent and reference plastic strain rate, respectively. T, T_{melt} and T_{room} are the work temperature, the material melting temperature and the room temperature, respectively. Material constants for the Johnson–Cook model are represented by n, m, A_1, B_1 and C_1, which are list in Table 1.

Table 1 Ti6Al4V constants for Johnson–Cook model

A_1[MPa]	B_1[MPa]	C_1	m	n	T_{melt}[℃]	T_{room}[℃]
1098	1092	0.014	0.93	1.1	1560	25

The cutter in this experiment is micro end-milling tools coated with ultra-fine tungsten. Figure 9 shows the SEM micro-image of the edge radius of flute, which is 5 μm. The clearance angle and the rake angle of the flute are 10 and 5 degrees, respectively.

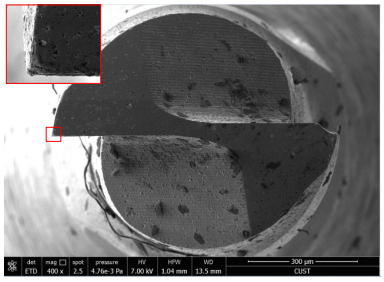

Figure 9 SEM of the micro end-mill tip

For this simulation, both sliding contact and sticking contact is applied to describe friction between the tool and the workpiece, as following [29]:

$$\begin{cases}\mu = 0.5\\ \tau_p = 500\ \text{MPa}\end{cases} \tag{23}$$

Where μ and τ_p are coulomb friction coefficient and maximum shear stress, respectively.

A series of FEM are performed at constant cutting speed 419 mm/s with different uncut chip thickness. The percent error in chip thickness per unit cutting length is less than 10%, which is associated with the accuracy of machine tool, tool-workpiece vibration and tool run out, etc. The simulated cutting forces per cutting width in the tangential and radial directions, F_t and F_r, are given in Figure 10.

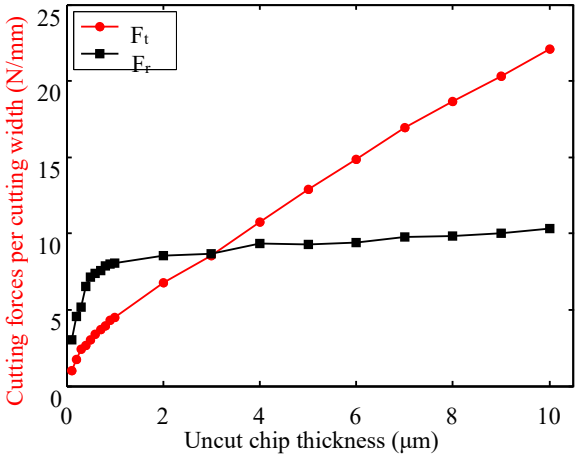

Figure 10 Cutting forces per cutting width variation from simulation

In order to consider both the ploughing and shearing effect in the cutting force model, the simulated cutting force variation curve vs. uncut chip thickness has covered the range of uncut chip thickness both greater than and less than minimum chip thickness. Subsequently, the determination of cutting force coefficients as functions of the uncut chip thickness has included both the ploughing and shearing effect, which will be calculated from cutting forces simulated by [13]:

$$K_t = \frac{\tau_s}{\sin\phi_n}\frac{\cos(\beta_n-\alpha_n)+\tan^2\eta\sin\beta_n}{\sqrt{\cos^2(\phi_n+\beta_n-\alpha_n)+\tan^2\eta\sin^2\beta_n}}$$

$$K_f = \frac{\tau_s}{\sin\phi_n\cos i}\frac{\sin(\beta_n-\alpha_n)}{\sqrt{\cos^2(\phi_n+\beta_n-\alpha_n)+\tan^2\eta\sin^2\beta_n}} \quad (24)$$

where ϕ_n, τ_s and β_n are the normal shear angle, shear stress and the friction angle, respectively. i and η are the inclination angle and the chip flow angle, respectively. The detailed calculation process of parameters is available from Ref. [21]. With cutting forces (F_t, F_r) obtained from FEM, the simulated cutting forces coefficient are shown in Figure 11.

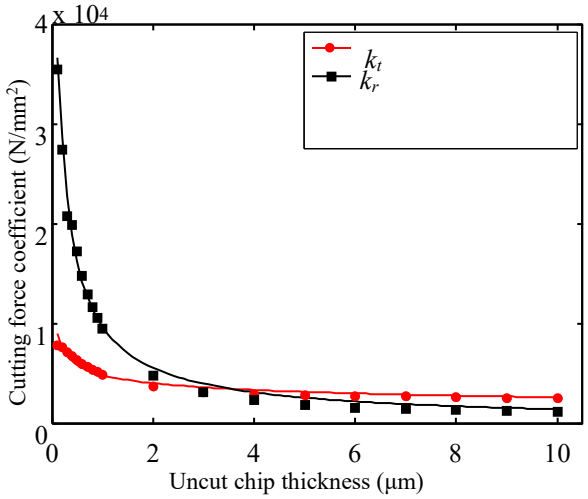

Figure 11 Non-linear fitting the cutting force coefficients

The minimum chip thickness is set as 0.8 μm in this study [24]. It can be seen in Fig.11 that the cutting force coefficient curve rises sharply due to the size effect when the uncut chip thickness is less than 1 μm, which is close to the minimum chip thickness. Therefore, the simulated cutting force coefficients can include ploughing coefficients related to elastic-plastic deformations of workpiece and shearing ones corresponding to chip formation. The cutting force coefficients as nonlinear function of the uncut chip thickness are fitted by:

$$\begin{cases} k_t = a_t \cdot h^{b_t} + c_t \cdot h^{d_t} \\ k_r = a_r \cdot h^{b_r} + c_r \cdot h^{d_r} \end{cases} \tag{25}$$

The parameters in Eq. 25 can be identified by curve-fitting date, and listed in Table 2

Table 2 Determined constants for the cutting force coefficients

a_t	b_t	c_t	d_t	a_r	b_r	c_r	d_r
744.420	-0.271	-8.855	69.377	21.073	-0.957	-1.135	-1.243

3. Experimental validation for the proposed model

3.1 Experimental setup

In order to validate the accuracy of the proposed model in section2, a series of micro end-milling experiments are conducted on A MAKINO-S33 precision CNC machining center, as shown in Figure 12. Ti-6Al-4V (TC4) with size of 60 mm×10 mm×3 mm is used in this tests. The cutter with two flute is used in this experiment, which is superfine tungsten steel coated TiAIN (SGO Co., Ltd, Taiwan) with HRC 55. The tool radius and helix angle are 0.8 mm and 35°, respectively. The experiment setup for tool run-out are depicted in Fig. 12(a). Two Keyence LK-H050 CCD laser-displacement sensors are applied to measure the tool run-out, the range and resolution of the CCD are 10 mm and 50 nm, respectively. Kistler type 9257B dynamometer is used to measure the cutting force in Fig. 12(b), whose sensitivity is 7.5 pC/N, 7.5 pC/N and 3.7 pC/N in the X-, Y- and Z-directions, respectively. A low-pass filter with a cut-off frequency of 500 Hz is employed to remove the high frequency noises in the experimental cutting force signals. The parameters for tool run out are obtained by the presented method in section 2.2. The detailed experimental conditions is summarized in Table 3.

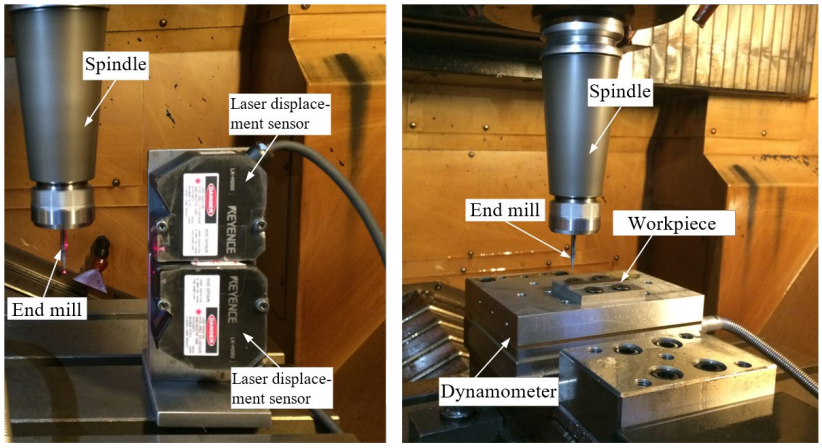

(a) Measure for run out (b) Measure for cutting force

Figure 12 Experimental setup

Table 3 The parameters setting for experiment with single factor and different series

Test series	Cutting parameters	level	unit
A	f_z	2.0/4.0/6.0/8.0	(μm/flute)
	d_a	0.06	(mm)
	ω	10,000	(rpm)
	$[\rho(0), \lambda(0)]$	[0.85,43.58]	(μm, deg)
B	f_z	2.0	(μm/flute)
	d_a	0.04/0.06/0.08/0.10	(mm)
	ω	10,000	(rpm)
	$[\rho(0), \lambda(0)]$	[0.85,43.58]	(μm, deg)
C	f_z	2.0	(μm/flute)
	d_a	0.06	(mm)
	ω	10,000	(rpm)
	$[\rho(0), \lambda(0)]$	[0.85,43.58][0.99,45.47]	(μm, deg)

3.2 Result and discussion

3.2.1 The cutting force with different feed per tooth

Figures 13 and 14 show comparisons of predicted and experimental cutting forces with different feed per tooth in the X- and Y-directions. It can be observed that the proposed cutting force model can well predict experimental results. Due to the presence of run-out, unequal two peaks appear in the profile of cutting force during one revolution. In addition, by comparing Fig.13 to 14, it can be observed that the effect of elastic recovery on predicted cutting force is more obvious for lower feed per tooth than that of higher feed per tooth, and the fluctuation on the cutting force in Y-direction is

more severe than that in the X-direction. Specifically, the maximum difference of peak-to-peak between experimental and predicted curves (Pe=0.2) are about 0.4 N in X- and 0.75 N in Y- direction at 2.0 μm/flute, respectively. However, the maximum difference of the peaks and the valleys between experimental and predicted curves (Pe=0.2) are about 0.2 N in X- and 0.3 N in Y- direction at 4.0 μm/flute, respectively. This is due to the underestimation of the tangential force from the FE model. It can be concluded that the cutter runout, tool-workpiece vibration and material elastic recovery have a significant effect on the cutting forces, especially at lower feed per tooth.

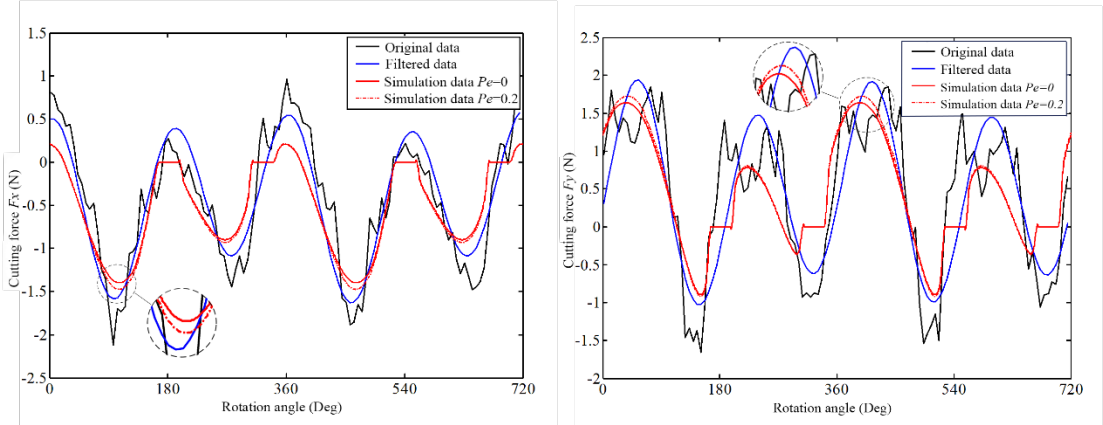

(a) X direction (b) Y direction

Figure 13 Predicted and experimental cutting forces with lower feed per tooth (serial A for 2.0 μm/flute)

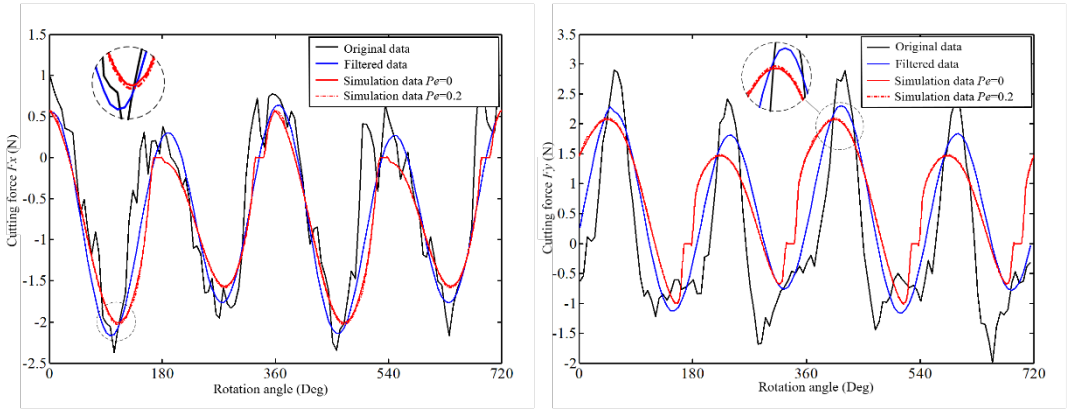

(a) X direction (b) Y direction

Figure 14 Predicted and experimental cutting forces with lower feed per tooth (serial A for 4.0 μm/flute)

To verify effectiveness of proposed model and investigate the effect of elastic recovery, the RMS values of the cutting force are calculated with different feed per tooth and elastic recovery (Pe=0 and 0.2). Comparison of RMS of predicted and experimental cutting forces in the X- and Y-directions with various feed per tooth are given in Figure. 15. It is obvious in Fig. 15 that the RMS

of cutting force increases with the increasing feed per tooth. The RMS of predicted cutting forces with the consideration of elastic recovery (Pe=0.2) shows a closer agreement with the experimental results as compared to those without the consideration elastic recovery (Pe=0). This phenomenon reveals that the elastic recovery has a significant effect on the predicted cutting force, especially at lower feed per tooth. Specifically, the errors RMS of cutting force predicted and experimental in X direction are 5.87% and 3.38% with consideration the elastic recovery at 2 μm and 4 μm feed per tooth, respectively, while those are 9.49% and 4.68% without consideration the elastic recovery, respectively. However, those in Y direction are 13.65% and 3.22% with consideration the elastic recovery at 2 μm and 4 μm feed per tooth, respectively, and 17.51% and 4.35% respectively without consideration the elastic recovery, respectively. It is noticeable that the maximum difference between experiments and simulation data with Pe=0 and Pe=0.2 is 17% and 13.65% in Y- direction at 2 μm feed per tooth, respectively. It might be due to deflection of the cutting tool, vibrations present in the machine tool at lower feed per tooth whose effects have not been considered in the present model. According to the analysis, it is obtained that the maximum error percentage between simulation and experiments is 13.65 % for the proposed cutting force model, the proposed model embedded the elastic recovery is improved for predicting cutting force, and predicted cutting force is more obviously affected by elastic recovery at smaller the feed per tooth.

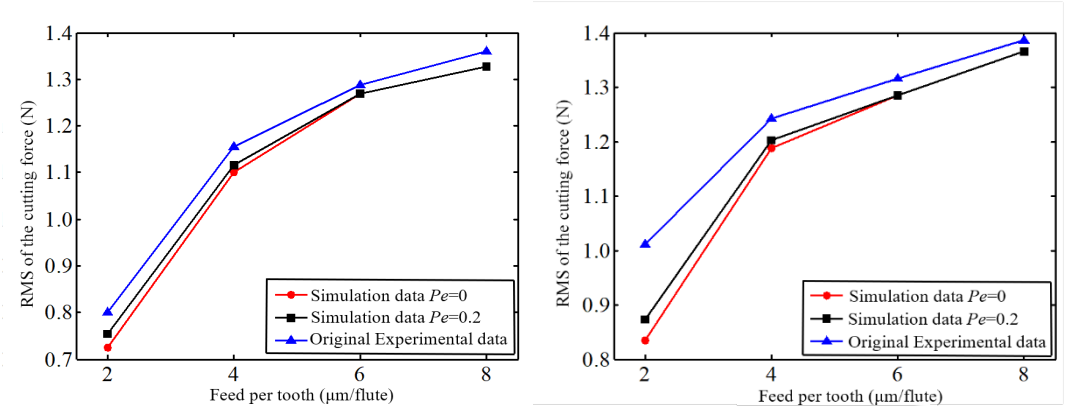

(a) X direction (b) Y direction

Figure 15 RMS value of the cutting force with various feed per tooth on (for serials A)

3.2.2 The cutting force with different depth of cut

Figure 16 show the comparison of RMS of predicted and experimental cutting forces with different cutting depths in the X- and Y-directions. It is obvious in Fig.16 that the proposed model can better

follow the law of RMS of experimental cutting force, the RMS of cutting force increases linearly with increasing the cutting depth. More specifically, the errors of RMS of experimental and predicted are 18.46%, 5.87%, 4.63% and 2.41% in X- direction, 13.62%, 13.65%, 4.36% and 1.77% in Y- direction at different cutting depths, respectively. Based on the analysis, the errors of experimental and predicted is getting smaller with increasing the cutting depth.

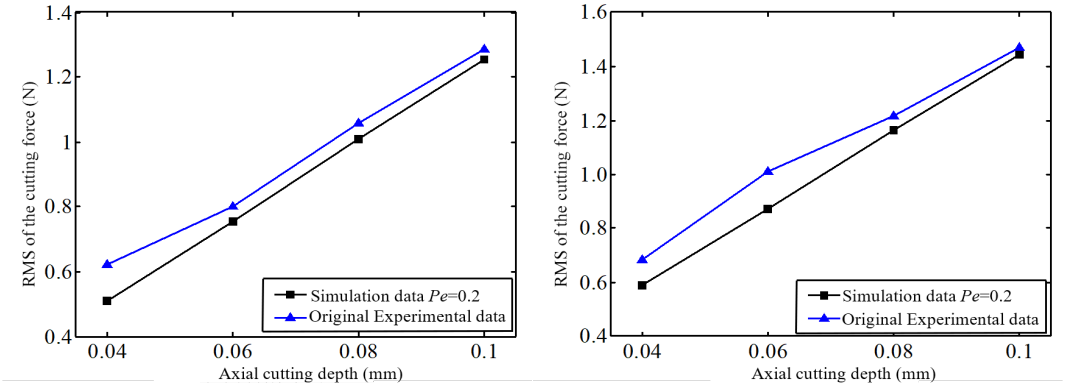

(a) X direction (b) Y direction

Figure 16 I RMS value of the cutting force with various depth of cut: (for serials B)

3.2.3 The cutting force with various tool run-out

As shown in Figures13 and 14, there are two unequal peaks in the cutting force signal during one revolution due to the presence of run-out. The comparison of experimental and predicted cutting force peak at different tool run-out is listed in Table 4. The tool run-out from test C-1 to C-2 change slightly, which result the peak of each flute changing greatly. More specifically, the ratios of peak experiment and simulation vary by 5.13% and 7.36% in X direction, while 2.24% and 4.07% in Y direction, respectively. Based on the analysis, it can be noted that the predicted model can better follow the trend of peak cutting force. In addition, the above results well demonstrate the importance of tool run-out calibration. The slight change of tool run-out will lead to a great variation in cutting force.

Table 4 The peak value comparison of cutting force with different tool run-out

No	Simulated [P_e=0.2] (N)		Experimental (N)	
	X direction	Y direction	X direction	Y direction
C-1	Peak1：1.476	Peak 1：1.725	Peak 1：1.585	Peak 1：1.938

	Peak 2：0.929	Peak 2：0.901	Peak 2：1.085	Peak 2：1.446
	Ratio：1.589	Ratio：1.915	Ratio：1.461	Ratio：1.340
	Peak 1：1.453	Peak 1：1.688	Peak 1：1.574	Peak 1：1.915
C-2	Peak 2：0.987	Peak 2：0.919	Peak 2：1.136	Peak 2：1.462
	Ratio：1.472	Ratio：1.837	Ratio：1.386	Ratio：1.310

4. Conclusions

In order to predict exactly cutting force, a mechanics model is comprehensively established by considering the variety of entry and exit angles for each engaged flute and an accurate instantaneous uncut chip thickness (IUCT) in this paper. The model of IUCT has considered the combination of the minimum chip thickness, tool run-out, and the material's elastic recovery. An experimental method is proposed to validate the accuracy of predicted cutting force. Based on the results, some conclusions can be obtained as following:

- The effect of elastic recovery rate on the IUCT relies on the feed per tooth and run out, which is more significant with smaller feed per tooth. Some abrupt changes appear in the value of IUCT due to the minimum chip thickness
- The cutting force coefficients as nonlinear function of the uncut chip thickness are obtained by a FEM method, which is sharply rising when the feed per tooth is less than or close to minimum chip thickness. The minimum chip thickness can be reflected by simulated cutting force coefficients, which is about 1μm in this study.
- The proposed model accurately provide prediction cutting force, and the effect of elastic recovery on predicted cutting force is more obvious at smaller the feed per tooth. The errors of experimental and predicted is getting smaller with increasing the cutting depth. The slight change of tool run-out will lead to a great variation in cutting force.

Acknowledgments

The first author would like to thank the financial support to this work by the National Key R&D Program of China (No. 2017YFB1104700), Program of International S&T Cooperation (No. 2016YFE0112100), National Natural Science Foundation of China (Nos. 51675376, 51675371, 51575380 and 51675367), and EU H2020 Program MNR4SCell (No. 734174).

Conflict of Interest

The authors declare that they have no conflict of interest.

References

1. Câmara M.A., CamposRubio J.C., Abrão A.M., Davim J.P. (2012) State of the Art on Micromilling of Materials, a Review, Journal of Materials Science & Technology 28(8): 673-685.
2. Sahoo Priyabrata, Pratap Tej, Patra Karali (2019) A hybrid modelling approach towards prediction of cutting forces in micro end milling of Ti-6Al-4V titanium alloy, International Journal of Mechanical Sciences 150(1): 495-509.
3. Choong Z.J., Huo D.H., Degenaar Patrick, O'Neill Anthony (2019) Micro-machinability and edge chipping mechanism studies on diamond micro-milling of monocrystalline silicon, Journal of Manufacturing Processes 38(2): 93-103.
4. Cho M.W., Kim D.W., Cho W.S. (2007) Analysis of micro-machining characteristics of Si3N4-hBN composites, J Eur Ceram Soc, 27 (2):1259-1265.
5. Arif M., Rahman M., San W.Y., Doshi N (2011) An experimental approach to study the capability of end-milling for microcutting of glass, Int J Adv Manuf Technol, 53 (9):1063-1073.
6. Zhang X, Ehmann KF, Yu T (2016) Cutting forces in micro-end-milling processes. International Journal of Machine Tools & Manufacture 107:21-40.
7. Srinivasa YV, Shunmugam MS (2013) Mechanistic model for prediction of cutting forces in micro end-milling and experimental comparison. International Journal of Machine Tools & Manufacture 67(2):18-27
8. Zhou YD, Tian YL, Jing XB, Ehmann KF(2017), A novel instantaneous uncut chip thickness model for mechanistic cutting force model in micro-end-milling, International Journal of Advanced Manufacturing Technology 93:2305-2319.
9. Oliveira FB, Rodrigues AR, Coelho RT, Souza AF (2015). Size effect and thickness in micromilling. International Journal of Machine Tools & Manufacture 89:39–54.
10. Bao WY, Tansel IN (2000) Modeling micro-end-milling operations. Part I: analytical cutting force model. International Journal of Machine Tools & Manufacture 40(15):2155-2173
11. Bao WY, Tansel IN (2000) Modeling micro-end-milling operations. Part II: tool run-out.

International Journal of Machine Tools & Manufacture 40(15):2175-2192

12. Vogler MP, Kapoor SG, DeVor RE (2004) On the modeling and analysis of machining performance in micro-endmilling, Part II: cutting force prediction. Journal of Manufacturing Science & Engineering 126(4):695-705

13. Park SS, Malekian M. (2009) Mechanistic modeling and accurate measurement of micro end milling forces. CIRP Annals - Manufacturing Technology, 58:49–52.

14. Jun MBG, Liu X, Devor RE, Kapoor Shiv G (2006) Investigation of the dynamics of microend milling-Part I: model development. Journal of Manufacturing Science & Engineering 128(4):893-900

15. Chen W.Q., Teng X.Y, Huo D.H., Wang Q.L. (2017) An improved cutting force model for micro milling considering machining dynamics. Int J Adv Manuf Technol 93:3005–3016

16. Yuan Y.J, Jing X.B, Ehmann Kornel, Cao J., Li H.Z., Zhang D.W., (2018) Modeling of cutting forces in micro end-milling, Journal of Manufacturing Processes 31, 844–858

17. Wan M., Wen D.Y., Ma Y.C., Zhang W.H., (2019) On material separation and cutting force prediction in micro milling through involving the effect of dead metal zone, International Journal of Machine Tools and Manufacture 146, 103452

18. Wojciechowski S., Matuszak M., Powałka B., Madajewski M., Maruda R.W., Krolczyk G. M., (2019) Prediction of cutting forces during micro end milling considering chip thickness accumulation, International Journal of Machine Tools & Manufacture 147, 103466

19. Thepsonthi T, Ozel T. (2015) 3-D finite element process simulation of micro-end milling Ti-6Al-4V titanium alloy: Experimental validations on chip flow and tool wear. Journal Material Process Technology 221:128–45.

20. Mittal RK, Kulkarni SS, Singh RK. (2017) Effect of lubrication on machining response and dynamic instability in high-speed micromilling of Ti-6Al-4V. Journal Manufacturing Processes, 28:413–421.

21. AltintasY. (2000) Manufacturing Automation, Cambridge University Press

22. Li H, Wu B (2016) Development of a hybrid cutting force model for micromilling of brass. International Journal of Mechanical Sciences (115-116):586-595

23. Jing XB, Tian YL, Yuan YJ, Wang F (2017) A runout measuring method using modeling and simulation cutting force in micro end-milling. International Journal of Advanced Manufacturing Technology 91(9-12) 1-11.

24. Malekian M, Park SS, Jun MBG (2009) Modeling of dynamic micro-milling cutting forces. International Journal of Machine Tools & Manufacture 49(7):586-598

25. Malekian M, Park SS, Um K (2008) Investigation of micro plowing forces through conical scratch tests.Transactions of SME-NAMRI 36(1):293-300

26. Gonzalo O, Jauregi H, Uriarte LG (2009) Prediction of specific force coefficients from a FEM cutting model. International Journal of Advanced Manufacturing Technology 43(3):348-356

27. Jing X, Li H, Wang J, Tian Y (2014) Modelling the cutting forces in micro-end-milling using a hybrid approach. International Journal of Advanced Manufacturing Technology 73(9):1647-1656

28. Rodríguez P, Labarga JE (2015) Tool deflection model for micromilling processes. International Journal of Advanced Manufacturing Technology 76(1):199-207

29. Segal J, Ratchev SM, Afazov SM. (2011) Determination of Cutting Forces and Process Stability in Micro-Milling of Ti6Al4V Alloy by Considering the Size-Effect Phenomenon. Micro & Nano systems 3(3): 199-209.